Supplementary Data for:

Evolution of calcite surfaces upon thermal decomposition, characterized by electrokinetics, in-situ XRD, and SEM

Matea Ban,[*,a,b] *Thomas Luxbacher,*[c,d] *Johannes Lützenkirchen,*[e] *Alberto Viani,*[f] *Sabrina Bianchi,*[b,g] *Klaudia Hradil,*[h] *Andreas Rohatsch,*[a] *and Valter Castelvetro* [b,g]

[a] Faculty of Civil Engineering, Research Centre of Engineering Geology, TU Wien, 1040 Vienna, Austria

[b] Department of Chemistry and Industrial Chemistry, University of Pisa, 56124 Pisa, Italy

[c] Anton Paar GmbH, 8054 Graz, Austria

[d] Faculty of Chemistry and Chemical Technology, University of Maribor, 2000 Maribor, Slovenia

[e] Institute for Nuclear Waste Disposal, Karlsruhe Institute of Technology, 76344 Eggenstein-Leopoldshafen, Germany

[f] Institute of Theoretical and Applied Mechanics of the Czech Academy of Sciences, 190 00 Praha, Czech Republic

[g] National Interuniversity Consortium of Materials Science and Technology (INSTM), 50121 Florence, Italy

[h] X-Ray Center, TU Wien, 1060 Vienna, Austria

CONTENTS

Figure S1 Permeability of the flow channel for the clamping cell 3

Table S1 Chemical composition as determined by XRF 4

Table S2 Mercury intrusion and helium-pycnometry analyses of AM 4

Figure S2a-d Micrographs before and after thermal treatment 5

Figure S3a-b SEM/EDX analysis to determine Ca-Si ratios 7

Figure S4-S5 XRD diffractograms 11

Figure S6 Structural evolution of quartz inversion observed by XRD patterns 14

Figure S7 ζ and pore conductivity of pristine and thermally treated calcite 15

Figure S8 Streaming current and streaming potential titration of LdA 16

Table S3 Summary of relevant properties for all testing conditions 18

Figure S9 Preparation of polypropylene for streaming current titration studies 20

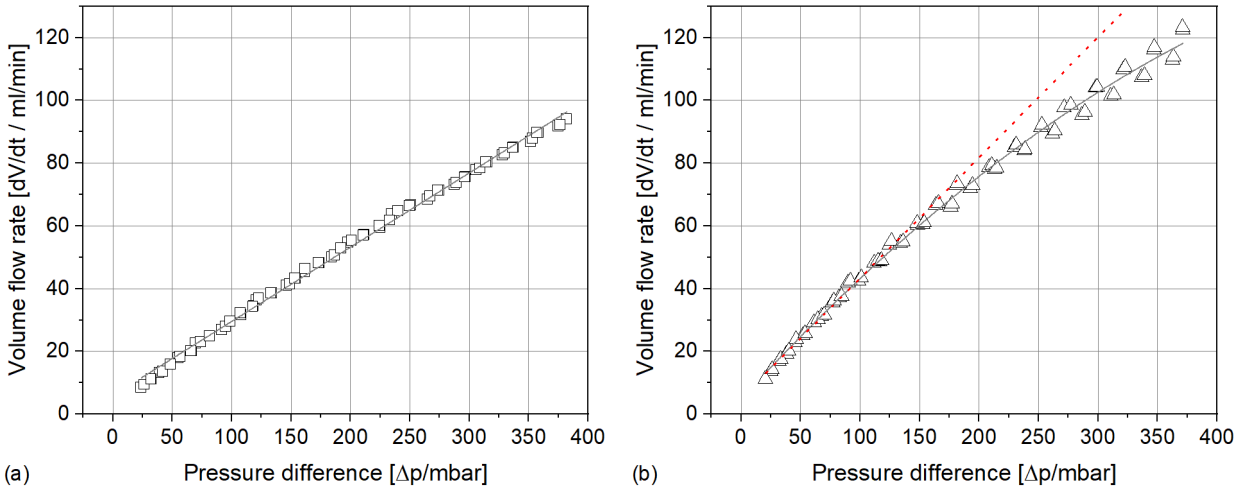

Figure S1. Permeability (volume flow rate vs. pressure difference) for the flow channel in the insert for axial core analysis of the SurPASS^{TM} clamping cell for **(a)** Apuan Marble and **(b)** Lumaquela de Ajarte. The tangent at $\Delta p \rightarrow 0$ mbar shown in (b) shows the slope for calculating the correct gap height. The linear regression of these data underestimates the gap height. The slope of the second-order polynomial fit describes the permeability of the flow channel more reliably. Note that both samples display an acceptable flow rate in both flow directions inside the channel.

Table S1. Chemical compositions determined through XRF and reported as wt.% for Apuan Marble (AM) and Lumaquela de Ajarte (LdA).

	Elemental Concentration [%]								
Sample	O	Ca	Si	Al	Mg	K	Fe	Na	P, Ti
AM	50.3	48.4	0.14	0.05	0.82	<0.05	<0.05	0.2	<0.01
LdA	51.21	45.44	1.37	0.75	0.48	0.34	0.2	<0.05	<0.05

X-ray fluorescence (XRF) was used to obtain information on chemical composition. The instrument used was a Panalytical AXIOS advanced PW4400/40.

Table S2. Mercury intrusion data for specimens in pristine and increasingly thermally treated conditions up to 700 °C for Apuan Marble. Prior to these tests, He-pycnometry (average of four measurements) was carried out on the same samples (1 cm^3 in size) to study changes in apparent skeletal density.

Name	Sample Conditioning	Hg-Porosity %	Density g/cm^3
AM Pristine	Sound	0.557	2.718 ± 0.001
AM 200°	200 °C	0.879	2.725 ± 0.011
AM 300°	300 °C	1.027	2.724 ± 0.009
AM 400°	400 °C	1.125	2.712 ± 0.001
AM 500°	500 °C	1.573	2.721 ± 0.001
AM 600° 1st cycle	600 °C 1st cycle	2.635	2.715 ± 0.000
AM 600° 3rd cycle	600 °C 3rd cycle	3.047	2.717 ± 0.000
*AM 700°	700 °C	10.625	2.699 ± 0.002

*Note that the sample named AM 700° has experienced massive degradation due to transformation processes, which is also indicated by the measured density.

Porometric properties were determined using the AutoPore IV 9500 (Micrometrics) device. The use of He-pycnometry (AccuPyc II 1340, Micromeritics) allowed the assessment of changes in apparent skeletal density when mineral transformation occurred upon thermal treatment.

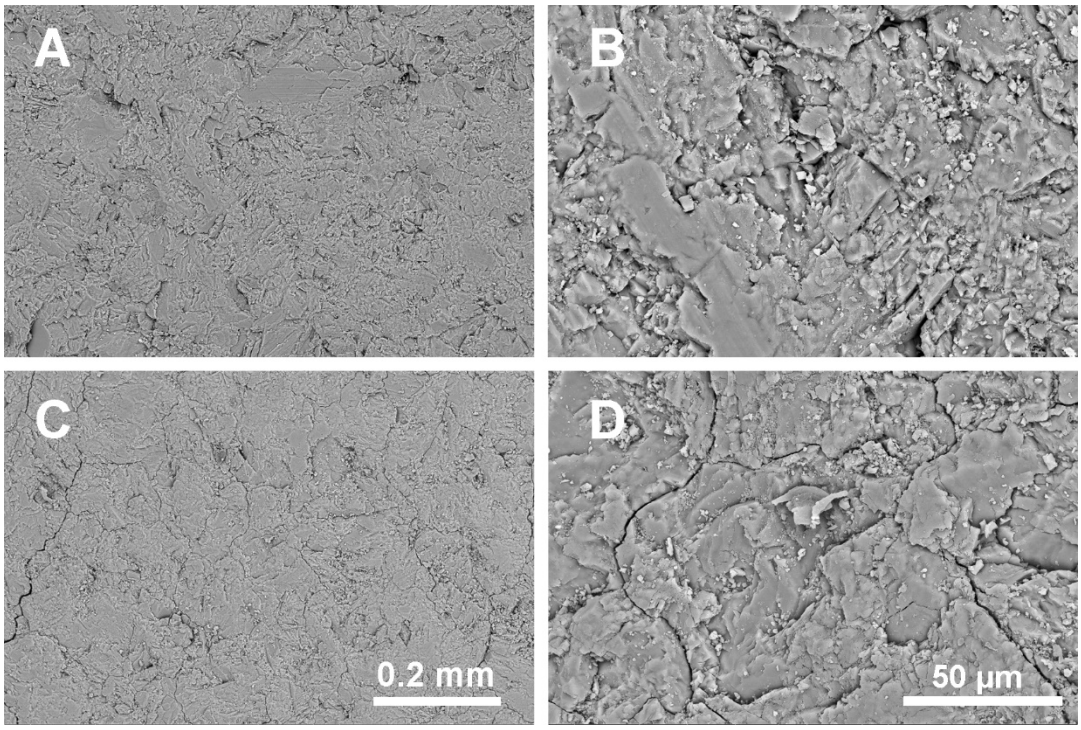

Figure S2a. Scanning electron microscopy micrographs taken with the concentric backscatter detector (CBS) before (**a** and **b**) and after thermal treatment (**c** and **d**) on surfaces of Apuan Marble.

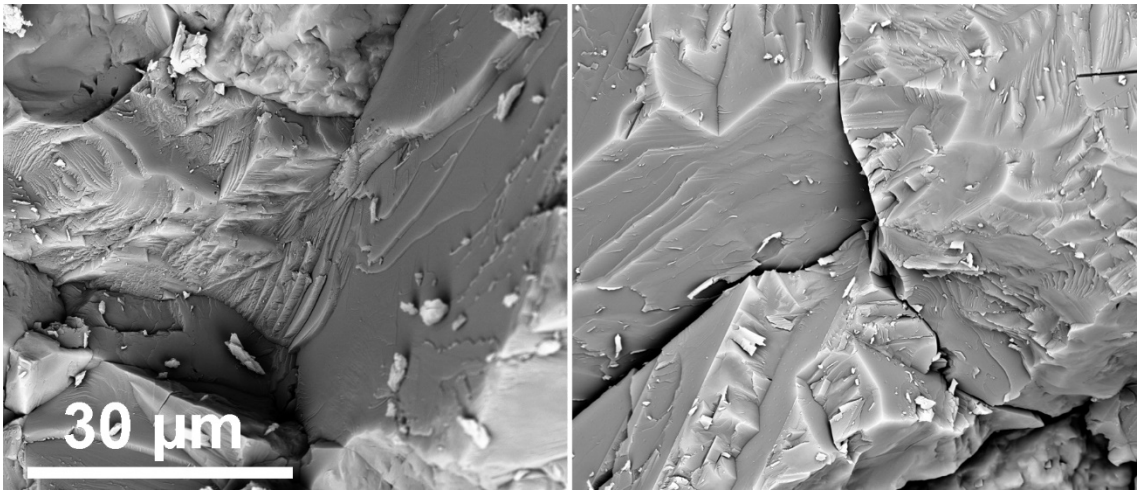

Figure S2b. Scanning electron microscopy micrographs of the BSED signal before (**left**) and after (**right**) thermal treatment on a chip (broken piece) of Apuan Marble exhibiting the loss of cohesion on a grain triple junction.

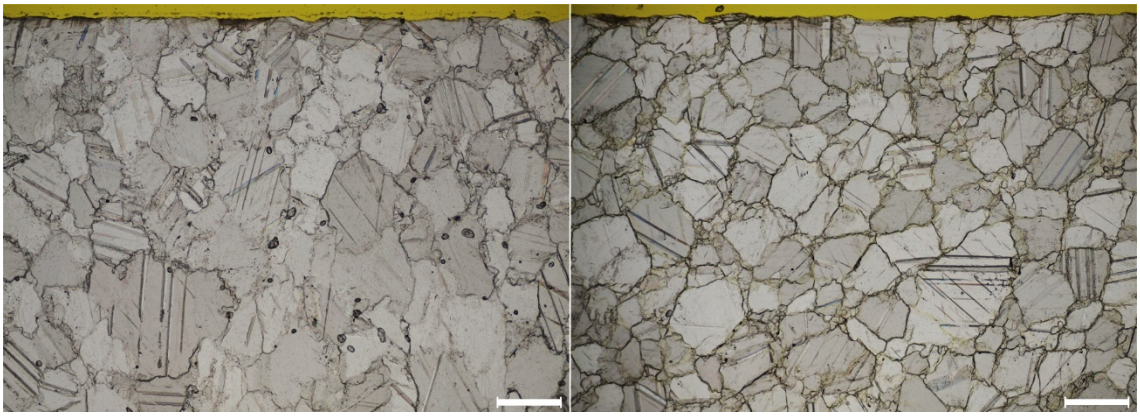

Figure S2c. Polarized microscope micrographs before **(left)** and after **(right)** thermal treatment of Apuan Marble. The fabric after thermal treatment displays mostly microcrack formation along grain boundaries. The scale bar is 200 μm.

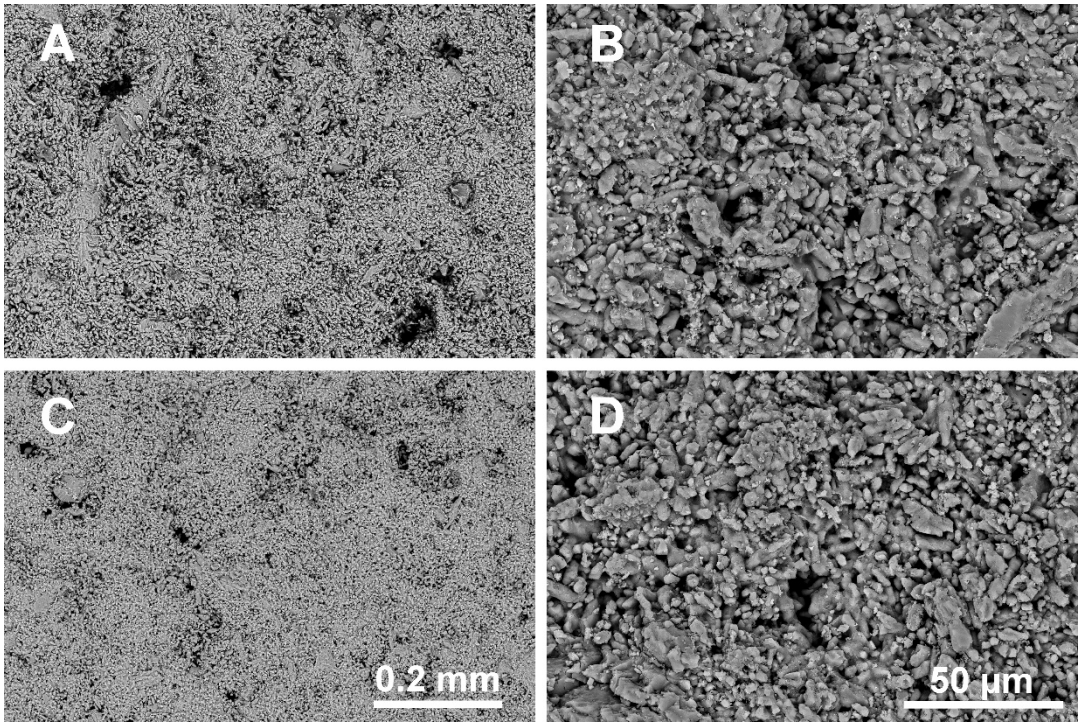

Figure S2d. Scanning electron microscopy micrographs taken with the concentric backscatter detector (CBS) before (**a** and **b**) and after thermal treatment (**c** and **d**) on surfaces of Lumaquela de Ajarte.

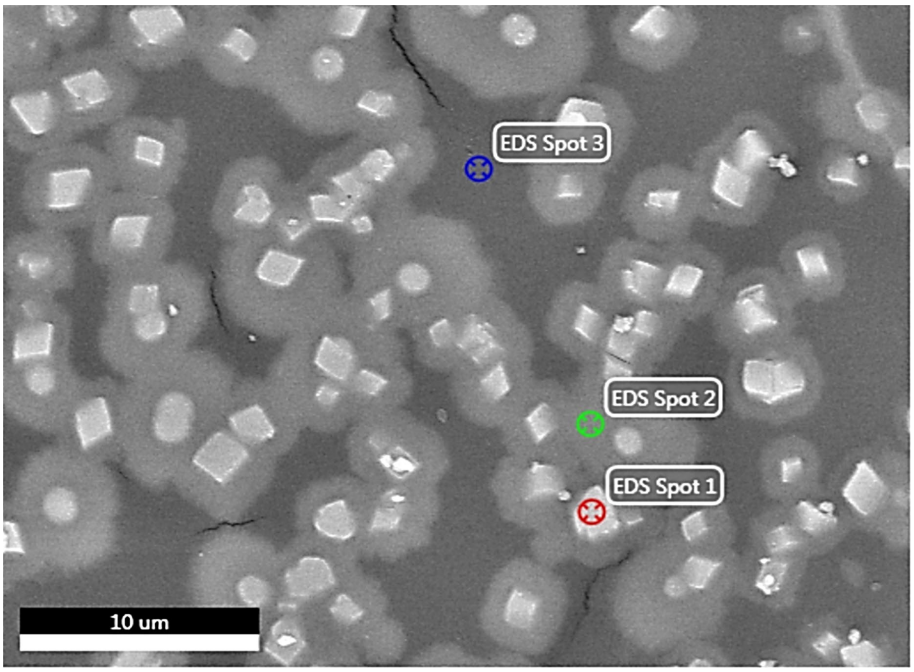
EDS Spot 3
EDS Spot 2
EDS Spot 1
10 um

(a)

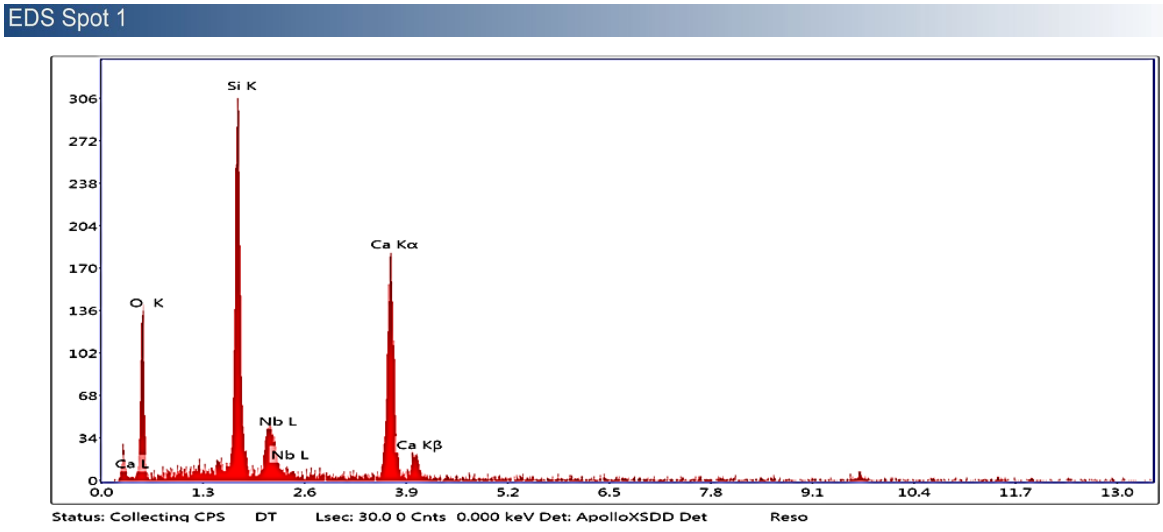
EDS Spot 1
Si K
Ca Kα
O K
Nb L
Nb L
Ca Kβ
Ca L
306
272
238
204
170
136
102
68
34
0
0.0
1.3
2.6
3.9
5.2
6.5
7.8
9.1
10.4
11.7
13.0
Status: Collecting CPS DT Lsec: 30.0 0 Cnts 0.000 keV Det: ApolloXSDD Det Reso

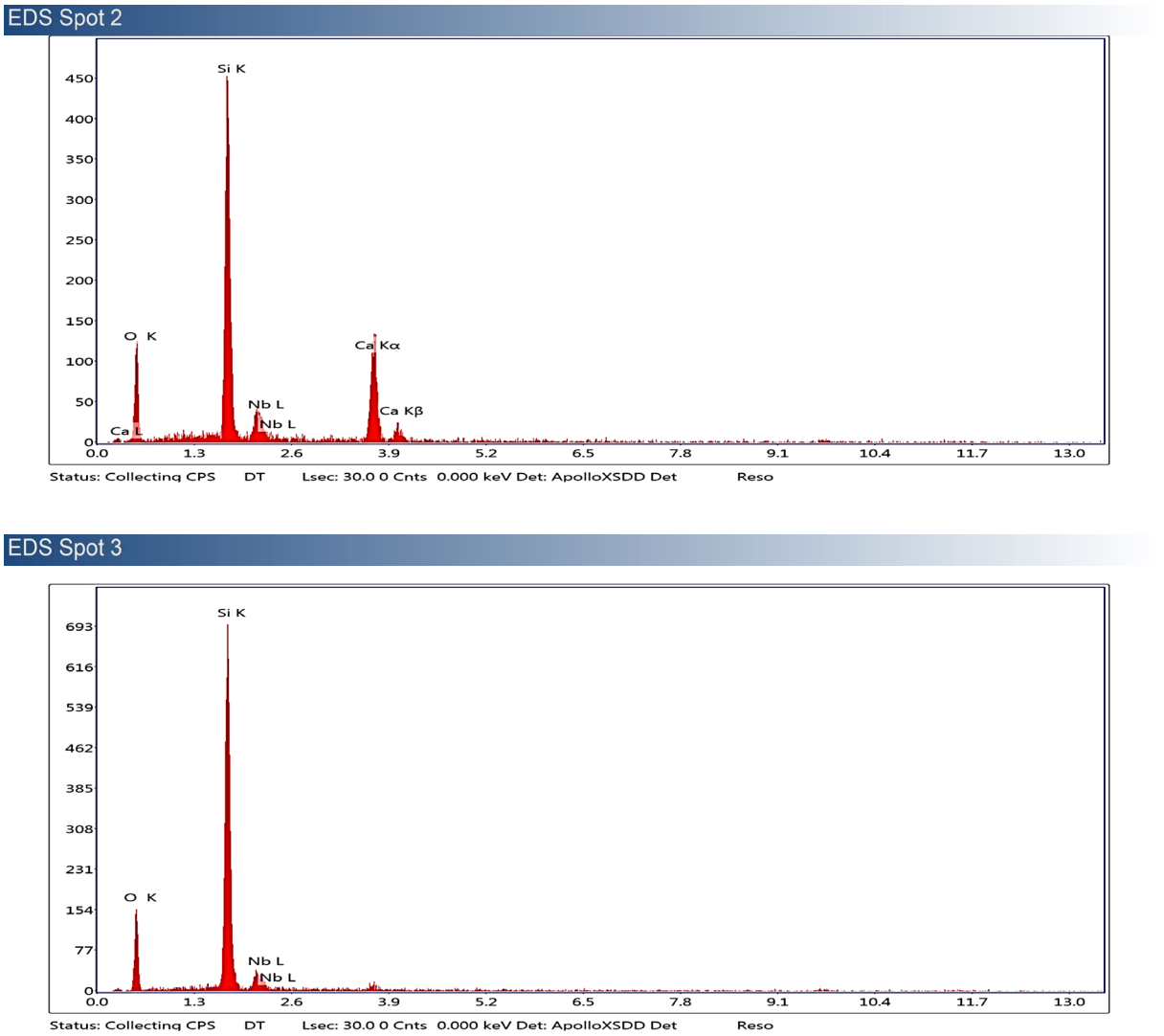

Figure S3a. SEM/EDX analysis of the whitish discoloration in the nanosilica consolidating matrix in Apuan Marble, revealing the distinguished intensities for Ca-Si ratios. The SEM micrograph was obtained in backscatter electron mode, highlighting the concentration gradients around the Ca-rich grains. EDX measurements were focused on the newly formed rhombohedrons (SPOT 1), on the white rim in the silica matrix surrounding the rhombohedrons (SPOT 2), and on the silica matrix surface (SPOT 3) with Apuan Marble as the substrate. The Nb signal is in fact an Au peak (as Au and Nb signals are close together, the software frequently mistakes Nb for Au), so it is present due to the conductive gold coating layer.

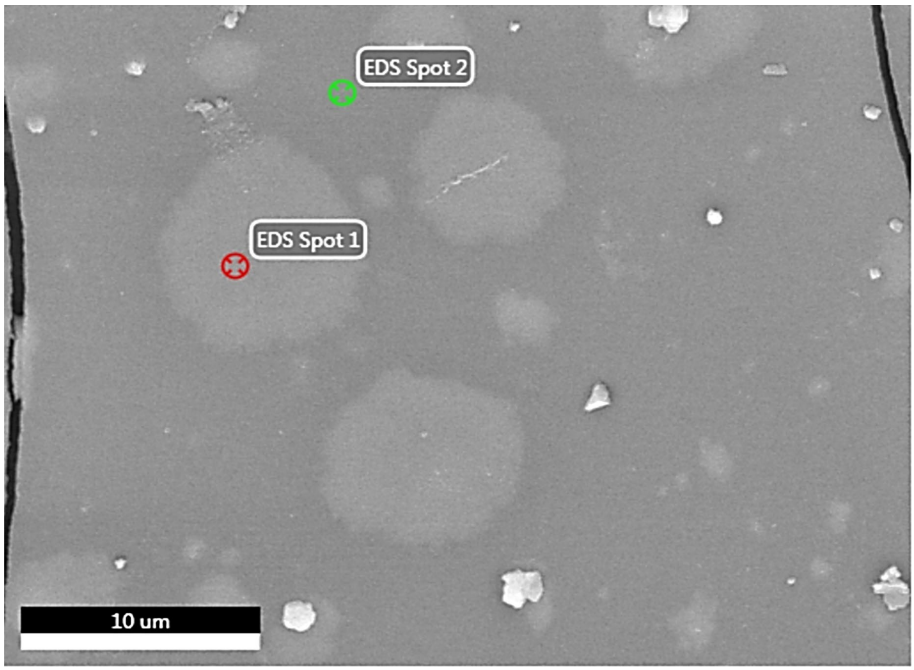
EDS Spot 2
EDS Spot 1
10 um

(b)

EDS Spot 1

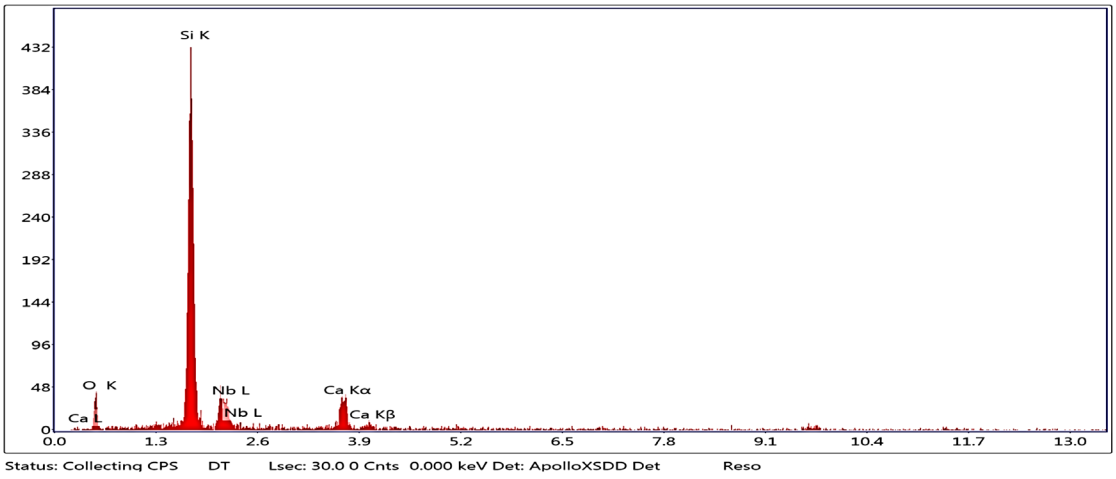
Si K
O K
Ca L
Nb L
Nb L
Ca Kα
Ca Kβ
432
384
336
288
240
192
144
96
48
0
0.0
1.3
2.6
3.9
5.2
6.5
7.8
9.1
10.4
11.7
13.0
Status: Collecting CPS DT Lsec: 30.0 0 Cnts 0.000 keV Det: ApolloXSDD Det Reso

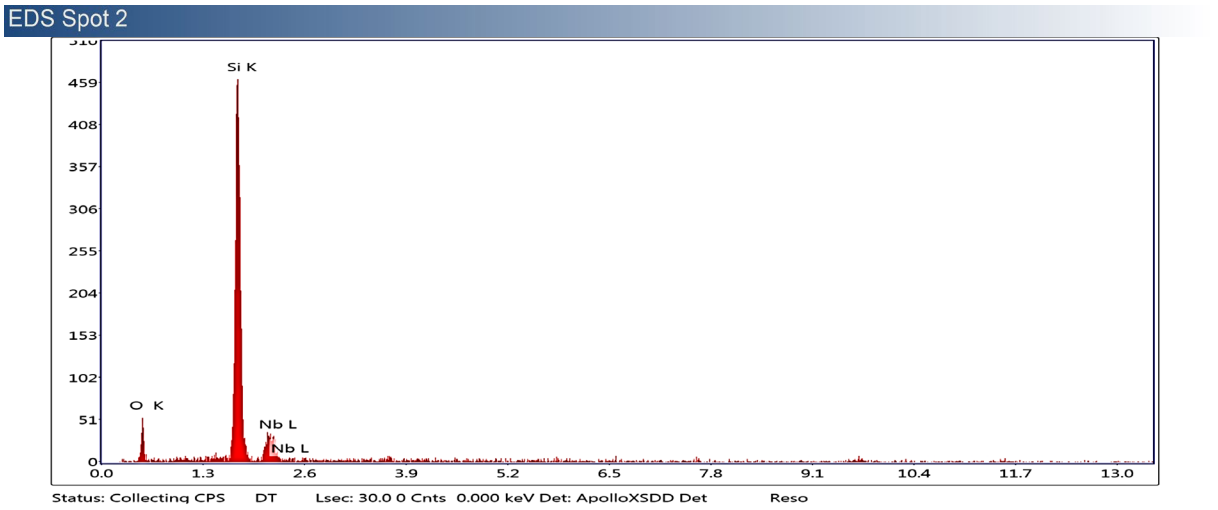

Figure S3b. Details of the SEM/EDX analysis of the whitish discoloration in the nanosilica consolidating matrix in Lumaquela de Ajarte, revealing the distinguished intensities for Ca–Si ratios. The SEM micrograph was obtained in backscatter electron mode. EDX analysis of the white rim present in the silica matrix (SPOT 1) and of the silica matrix (SPOT 2).

Exemplary XRD Diffractograms

The weight fraction of each of the phases in the samples was obtained adopting the Rietveld method, in which the difference between the experimental XRD diffraction profile and the calculated one is minimized through a least-squares procedure. Typically, during the Rietveld refinement for quantitative phase analysis, the background, some parameters of the peak profile shape, the weight fraction and the parameters of the unit cell of each phase are left free to change, in order to match the experimental diffraction pattern and account for variations, such as those induced by temperature changes (thermal expansion). Few characteristic diffractograms (with measurements performed with constant wavelength) are shown below. Note that the difference in peak position between the spectrum collected at 35 °C and the others is due to the thermal expansion.

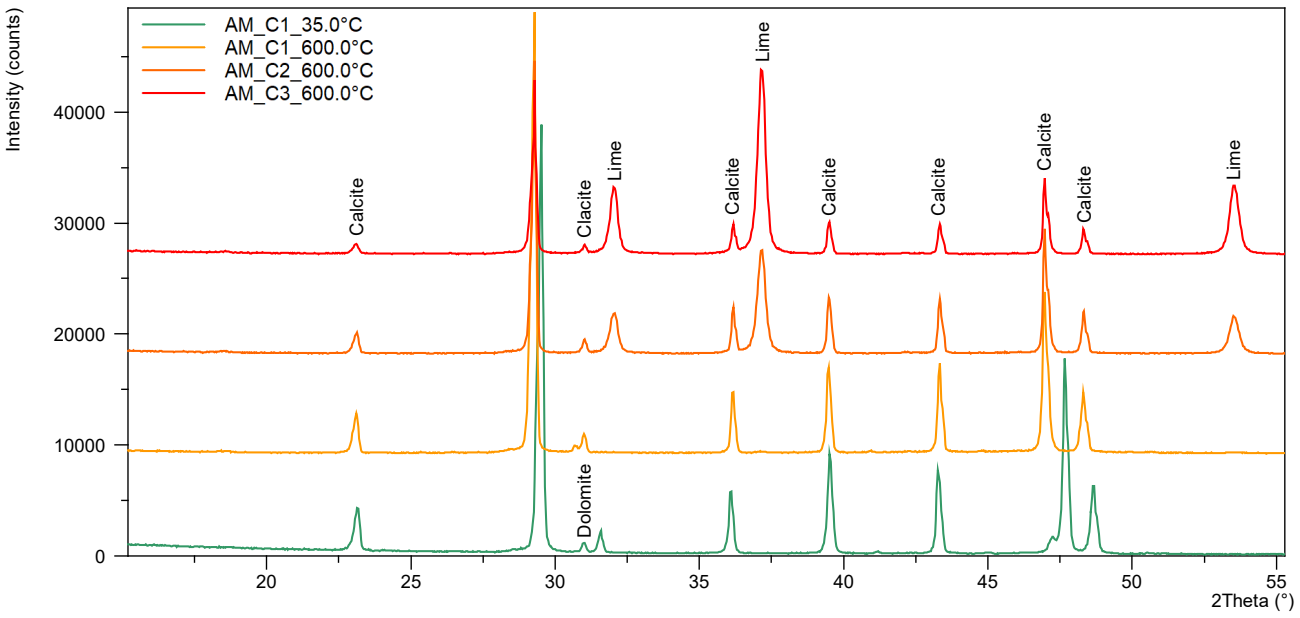

(a)

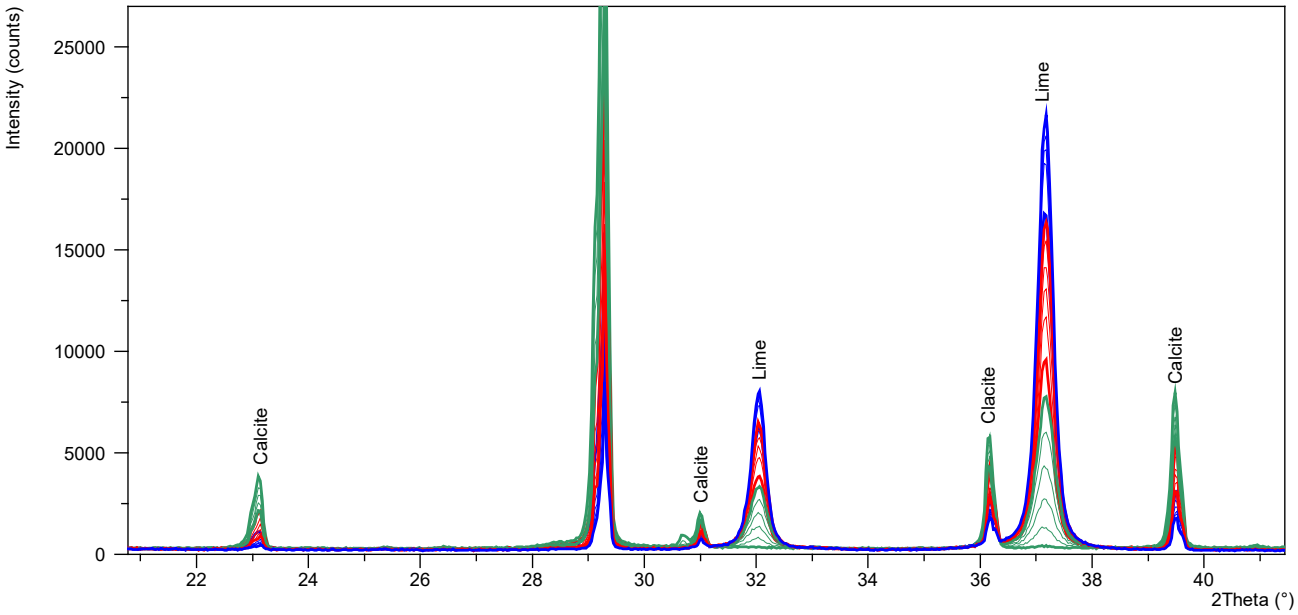

(b)

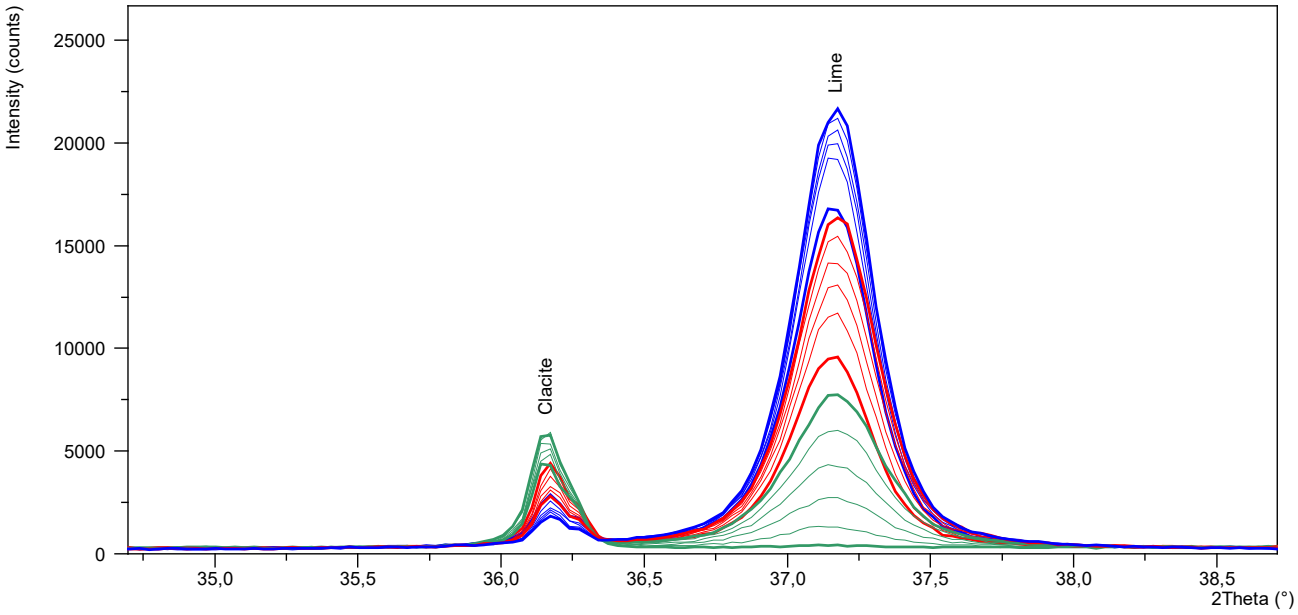

(c)

Figure S4. (a) Apuan Marble diffractograms collected at 35 °C and the first patterns (out of six) collected during the isothermal condition at 600°C per cycle exposed. **(b)** and **(c)** Overview and detail of Apuan Marble diffractograms as analyzed by in-situ XRD at isothermal conditions at 600 °C (corresponding to six patterns per cycle). Displayed is the decomposition of calcite and formation of calcium oxide through the cyclic thermal treatments (**green:** 1st isothermal cycle at 600°C, **red:** 2nd isothermal cycle at 600°C and **blue:** 3rd isothermal cycle at 600 °C).

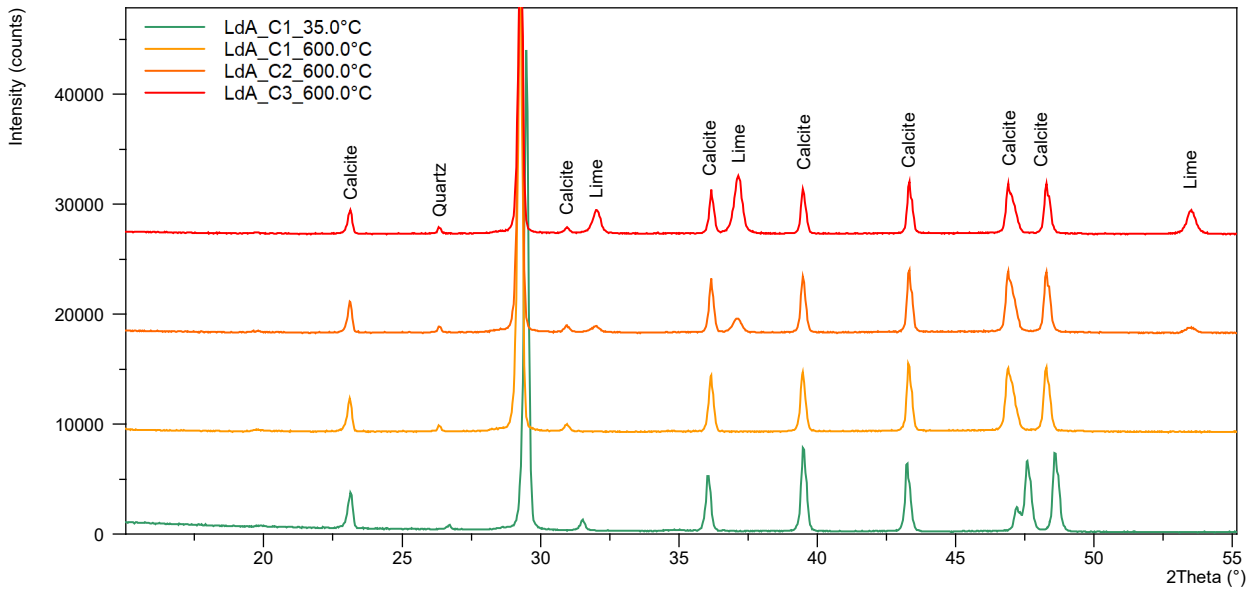

(a)

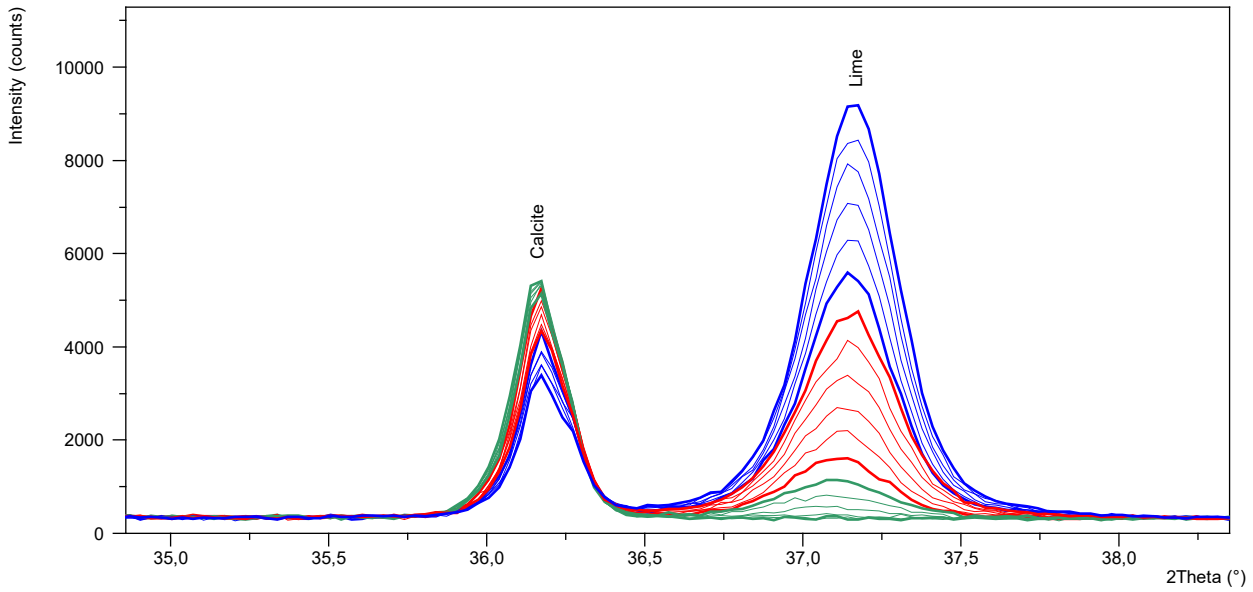

(b)

Figure S5. (a) Lumaquela de Ajarte diffraction patterns collected at 35 °C and the first patterns (out of six) collected during the isothermal condition at 600°C per cycle exposed. **(b)** Detail of Lumaquela de Ajarte diffractograms as analyzed by in-situ XRD at isothermal conditions at 600 °C (corresponding to six patterns per cycle). Displayed is the decomposition of calcite and formation of calcium oxide through the cyclic thermal treatments (**green:** 1st isothermal cycle at 600°C, **red:** 2nd isothermal cycle at 600°C and **blue:** 3rd isothermal cycle at 600 °C).

Note that the quartz reflections do not disappear but they are shifted slightly towards lower angle in the high temperature regime (**Figure S5a**). To illustrate the changes better we include the difference of low to high quartz in a separate pattern:

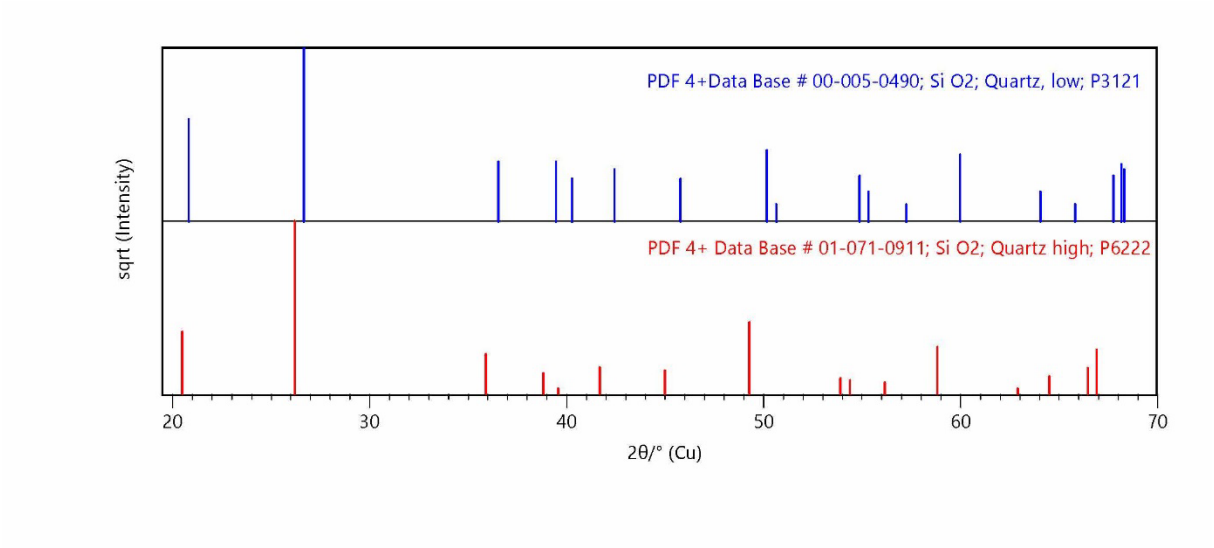

Figure S6. The structural evolution of quartz inversion as observed by XRD patterns

Interatomic distances are correlated with unit cell lattice parameters and employing higher temperatures results in changes of these interatomic distances, which is reflected in the change of the peak position. In the case of quartz two forms are distinct, the alpha- or low quartz that is stable until 573 °C and the beta- or high quartz that is stable above 573 °C [1]. There are no further transformations that occur up to 600 °C. The transition from low- to high quartz is a sudden phase transition (change in crystal structure due to displacement but no bonds are broken [2]) accompanied by a linear expansion. This linear expansion, along with the linear expansion of calcite, is what is responsible for the variations as analyzed by Rietveld refinement (<1 wt.%). The expansion of the minerals causes changes in the penetration depth of the X-rays, which adds to the fluctuation in qualitative analysis. Please note that the specimen displacement was corrected through solving the lattice parameter in each diffractogram.

ζ and Pore Conductivity of Pristine and Thermally Treated Calcite

The electrokinetic properties of the carbonates were studied in their pristine and thermally treated conditions also by employing single-point measurements, as shown in **Figure S7**. A significant difference between the apparent and corrected ζ values obtained from streaming potential measurements, ζ-App(U_{Str}) and ζ-Corr(U_{Str}), respectively, is prominent in all studied conditions for LdA, while it is significant (i.e., beyond the range of experimental error) only for the thermally treated samples in the case of AM. The resulting differences highlight the necessity of corrections for the effect of pore conductivity. The reason for the difference between ζ-App(U_{Str}) and ζ-Corr(U_{Str}) for the thermally treated ($Aged_{24}$ and $Aged_{365}$) AM is the newly formed microcracks. Unlike AM, LdA does not exhibit alterations after thermal treatment, which is in agreement with the limited change in porosity (**Figure S2d** and porometric data from the corresponding manuscript). The higher the porosity, the more severe the underestimation of ζ as determined by streaming potential. The pore conductivity causes an underestimation of ζ-Corr(U_{Str}) values by approx. 90% in the case of the highly porous LdA for all studied conditions and up to 20% for the pristine dense AM. After the formation of microcracks, the underestimation of ζ-Corr(U_{Str}) for the thermally treated AM increases to ~70%. It should be noted that pH-dependent data exhibit the same underestimation of ζ due to effects of pore conductivity as can be seen in **Figure S8**.

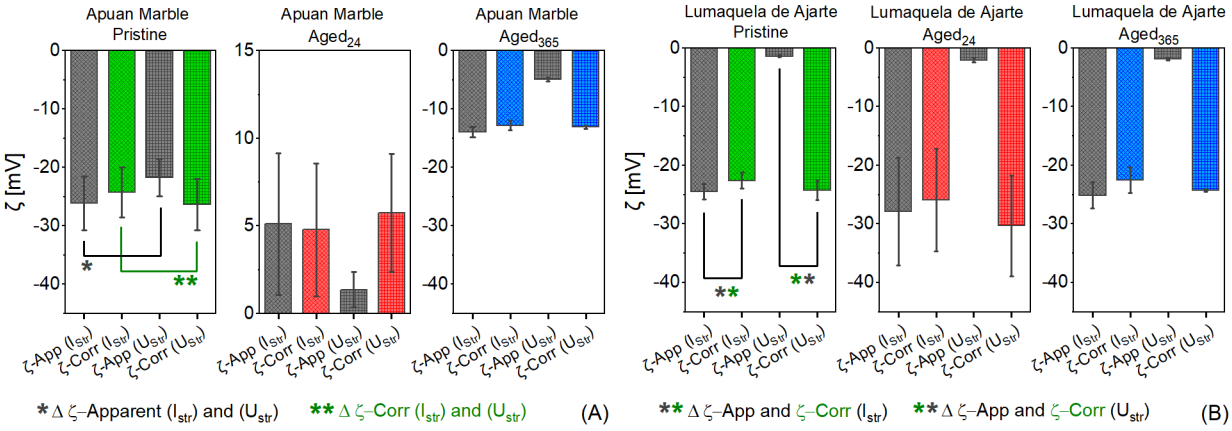

Figure S7. Apparent and corrected (to account for permeability and pore conductivity) ζ-potential values as obtained by streaming current (I_{str}) and streaming potential (U_{str}) measurements under nonequilibrium conditions and neutral pH using a 10^{-3} M KCl probing solution. Measurements performed with a CC cell on pristine and thermally treated ($Aged_{24}$, $Aged_{365}$) surfaces of **a)** Apuan Marble and **b)** Lumaquela de Ajarte. The pH was varied stepwise from 7.5 to 7.7 for Apuan Marble and from 7.5 to 8.2 for Lumaquela de Ajarte.

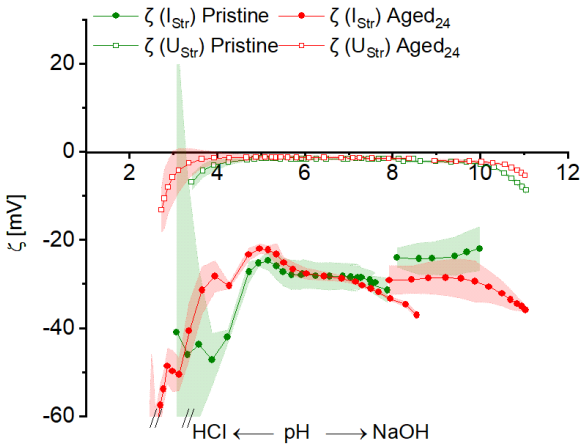

Figure S8. Streaming current (I_{str}) and streaming potential (U_{str}) titration in the 3 < pH < 11 range performed on pristine and thermally treated ($Aged_{24}$) surfaces of Lumaquela de Ajarte, as analyzed in the CC configuration (N_2-purged 10^{-3} M aqueous KCl probing solution), to assess the influence of pore conductivity on ζ-U_{str} readings. The resulting differences highlight the necessity for corrections of the effect of pore conductivity.

For AM in its pristine state, both ζ-Corr(I_{Str}) and ζ-Corr(U_{Str}) yield values of −25 mV ± 4 mV. However, upon thermal treatment, they become positive (5 mV ± 4 mV). The thermally altered surface contains a fraction of highly reactive CaO that quickly hydrates as it comes into contact with the aqueous solution, resulting in positive electrokinetic charge as a consequence of partial hydroxide ionization and the release of hydroxyl ions, leaving a surface excess of calcium cations. These results indicate that reactive phases, when present, may govern electrokinetic charge, even when the surface coverage of the reactive phases is below 50% (note that half of the microchannel inner surface is made of PP and the other half is a mixed system of calcite and calcium (hydr)oxide). Different contributions to electrokinetic charge for mixed systems may involve the combined effects of both higher reactivity and larger effective surface area. Nevertheless, the present measurements were well reproducible, even for these nonequilibrium conditions. A shift in the electrokinetic charge to positive ζ values was detected for the freshly aged AM, as it re-carbonates less rapidly than LdA. Upon re-carbonation, the electrokinetic charge of AM changes sign again, yielding ζ-Corr(I_{Str}) and ζ-Corr(U_{Str}) of −13 mV. The observed difference between the average ζ-Corr for AM in its pristine and re-carbonated states can be partially explained by the more effective release of lattice ions after thermal treatment and

re-carbonation (increased adsorption of Ca^{2+} yields more positive ζ values, source of ions is calcite dissolution) and due to the absence of organic matter (organic matter yields more negative ζ values when present). The decrease in the electrical resistance inside the streaming channel gives additional evidence for the thermally altered surfaces being more prone to dissolution (see cell resistance values in **Table S3**), as the interface between the bulk substrate and the phase-transformed/re-precipitated deposits is known to be a weakly bound layer prone to cracking and detachment.

For LdA, ζ-Corr(IStr) and ζ-Corr(UStr) remain comparable in magnitude at around −25 mV for all studied conditions, with the samples Aged24 exhibiting the greatest scattering (± 8.5 mV). Although organic matter may have an influence on the electrokinetic charge of pristine carbonates, making it more negative [3], such influence can be excluded for the surfaces exposed to cyclic heating at 600 °C, which results in the pyrolytic removal of all contaminating organic matter for both freshly thermally treated and re-carbonated samples. Similarly, trace-element incorporation that may affect ζ [4] can be disregarded in the present study, as shown by the substantial invariance of ζ to thermal ageing of the less-pure LdA, i.e., that containing iron oxide-hydroxides which undergo a thermally induced phase transformation [5,6] that is being irrelevant for ζ as it is only present at <1 wt.% (see chemical composition in **Table S1**).

Table S3. Summary of relevant properties for all testing conditions of Apuan Marble (AM) and Lumaquela de Ajarte (LdA) as determined in the asymmetric cell configuration (CC) and the symmetric cell configuration (AGC).

Carbonate (Cell type)	Condition[(1)]	Testing mode	ζ-I_{str} and ζ-U_{str} [mV][(2)]	Testing pH	IEP_{pH}[(3)]	Gap Height [μm][(4)]	κ_B [mS/m]	Cell Res. [kOhm][(5)]
AM (AGC)	Pristine Non-Eq	Time-resolved (62.5 h)	I_{str} −19.5 ± 1.6 to −10.1 ± 0.3 U_{str} −18.9 ± 1.9 to −9 ± 0.4	7 to 8.6	n/a	141	20.3 (±1.5)	623 (±53.3)
LdA (AGC)	Pristine Non-Eq	Time-resolved (1.3 h)	I_{str} 5.5 ± 3.6 to −5.1 ± 1.9 U_{str} 1.6 ± 0.3 to −1.3 ± 0.2	8.2 to 9.1	8.9	137	17.1 (±0.5)	151 (±1)
AM (CC)	$Aged_{1.5}$ Non-Eq	Time-resolved (8 h)	I_{str} 45.3 ± 9.5 to 5.0 ± 16.4 U_{str} 5.9 ± 3.1 to 1 ± 1.6	9.7 to 9.6	~9.8	118	20.7 (±0.8)	170 (±27.9)*
LdA (CC)	$Aged_{1.5}$ Non-Eq	Time-resolved (15 h)	I_{str} 18 ± 13 to −6.5 ± 1.3 U_{str} 6.9 ± 6.4 to −0.7 ± 0	6.7 to 9.6	~9.6	113	17.7 (±1.2)	139 (±1.9)*
AM (CC)	Pristine Non-Eq	Titration and single point	−25.3 ± 4.5	7.5 ± 0.2	3.4	132	19.5	1164 (±44.5)
AM (CC)	$Aged_{24}$ Non-Eq	Titration and single point	5.3 ± 3.6	7.6 ± 0.2	11	128	20.3	310 (±43)
AM (CC)	$Aged_{365}$ Non-Eq	Titration and single point	−12.9 ± 0.2	7.7 ± 0.1	4.6	141	17.8	453 (±1.2)
LdA (CC)	Pristine Non-Eq	Titration and single point	−23.4 ± 1.7	7.8 ± 0.3	n/a	103	21.8	88 (±7.2)
LdA (CC)	$Aged_{24}$ Non-Eq	Titration and single point	−28.1 ± 8.9	8.2 ± 0.2	n/a	110	21.9	101 (±11.3)
LdA (CC)	$Aged_{365}$ Non-Eq	Titration and single point	−23.4 ± 0.9	7.6 ± 0.2	n/a	128	22	102 (±0.4)
AM+PP (AGC)	Pristine Non-Eq	Titration and single point	–28 to –33	7.9	5.6	148	17.1	680 (±10)
PP (AGC)	Pristine	Titration and single point	–50 to –55	5.8	4.8	115	15.9	785 (±11)
AM (AGC)	Pristine Non-Eq	Titration and single point	–16 to –19	8.9	5.9	107	17.8	1105 (±13)
PP (CC)	Pristine	Titration and single point	–49	5.8	4.6	105	16.2	1088 (±2)

(1) Open system and N_2 purged during experiments. Time passed prior to recording was approx. 5 min, which is necessary to assure a complete wetting of the surface and conditioning for the flow rate measurement. If not stated otherwise, the initial pH of the 1 mM KCl aqueous electrolyte corresponded to approx. 5.5-6.5 due to the use of ultrapure water.

(2) Average ζ-(Corr) values, otherwise time-resolved experiments with first and last recording reported.

(3) Obtained either through titration or time-dependent streaming.

(4) The channel dimensions were corrected from a width of 5 mm and the length of 25 mm to a width of 6 mm and the length of 12.5 mm due to the use of a custom-made microchannel in the CC configuration.
(5) The listed cell resistance inside the streaming channel corresponds to the shift from ζ-Istr to ζ-Ustr measurements in single-point mode or to the change from the beginning to the end of the experiments for time-resolved mode. Note that the decrease in cell resistance inside the streaming channel indicates ion accumulation, which can be correlated with porosity (compare AM and LdA or compare AM-Pristine to AM-Aged) and help to account for effects of pore conductivity when streaming potential measurements are obtained. Moreover, changes in cell resistance during the experiments might indicate the reactivity of the sample.

*First recording excluded

Preparation of Polypropylene for Streaming Current Titration Studies

Preparation of the Polypropylene (see **Figure S9**) was done by cutting and grinding the surface with an abrasive paper. To exclude any leaching the surfaces were rinsed with a 0.1 M HCl and 0.1 M NaOH. Subsequently, ethanol was employed to clean the surfaces followed by multiple ultrasonic baths in ultra-pure water.

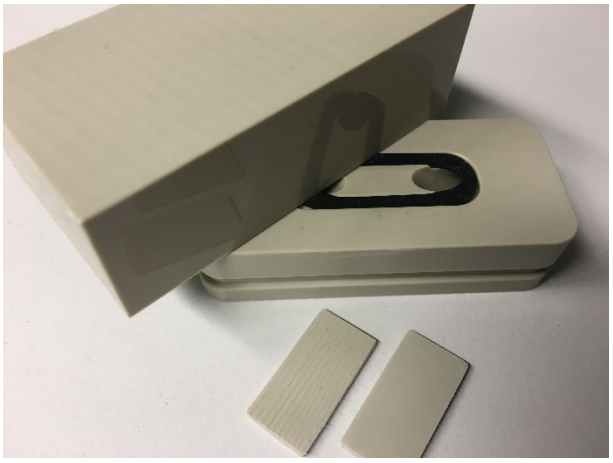

Figure S9. Preparation of the PP

References

[1] Britannica, T. Editors of Encyclopaedia (2020). Quartz. Encyclopedia Britannica. https://www.britannica.com/science/quartz

[2] Simmons, W. B. and Stewart, David B. (2018). Silica mineral. Encyclopedia Britannica. https://www.britannica.com/science/silica-mineral

[3] L. Madsen, Calcite: surface charge, Encyclopedia of surface and colloid science, CRC Press 2015, pp. 801-813.

[4] M. Wolthers, L. Charlet, P. Van Cappellen, The surface chemistry of divalent metal carbonate minerals; a critical assessment of surface charge and potential data using the charge distribution multi-site ion complexation model, Am. J. Sci., 308 (2008) 905-941.

[5] E. Brendle, J. Dentzer, E. Papirer, Variation of the surface properties of hematite upon heat treatment evidenced by inverse gas chromatography and temperature programmed desorption techniques: Influence of surface impurities and surface reconstruction, J. Colloid Interface Sci., 199 (1998) 63-76.

[6] A.F. Gualtieri, P. Venturelli, In situ study of the goethite-hematite phase transformation by real time synchrotron powder diffraction, Am. Mineral., 84 (1999) 895-904.